First publ. in: Physical Review Letters 105 (2010), 066402
DOI 10.1103/PhysRevLett.105.066402

Supplementary material to *"Disentanglement of the electronic and lattice parts of the order parameter in a 1D Charge Density Wave system probed by femtosecond spectroscopy"*

H. Schäfer[1], V. V. Kabanov[2,3], M. Beyer[1], K. Biljakovic[4], and J. Demsar[1,2,3]

[1]Physics Department and Center of Applied Photonics, Universität Konstanz, D-78457, Germany

[2]Zukunftskolleg, Universität Konstanz, D-78457, Germany

[3]Complex Matter Department, Jozef Stefan Institute, SI-1000, Ljubljana, Slovenia

[4]Institute of Physics, Hr-10000 Zagreb, Croatia

Contents

1. Experimental Set-up

The data were recorded using the experimental set-up, whose simplified scheme is shown in Fig. 1. The incoming beam (800 nm, 50 fs, 250 kHz) is split into a pump and a probe arm using a beam splitter. We utilize the so called fast scan technique, where the time-delay between the pump and the probe pulse is delayed via a mechanical shaker. The shaker operates at a frequency of about 20 Hz, and its maximum displacement corresponds to the time delay of 100 ps. To achieve larger time delays, as in the present experiment, we use an additional computer controlled delay stage in the pump arm, enabling a maximum time delay of 4 ns. We use the differential detection scheme (the signal from the beam reflected from the sample's surface is subtracted from the reference beam) and averaging on the oscilloscope to achieve high signal-to-noise ratio. The pump beam has been focused down to a 100 μm diameter spot with a 300 mm lens, while the probe beam is focused with a 150

mm lens to a spot with a 50 µm diameter to ensure probing of a homogenously excited sample area.

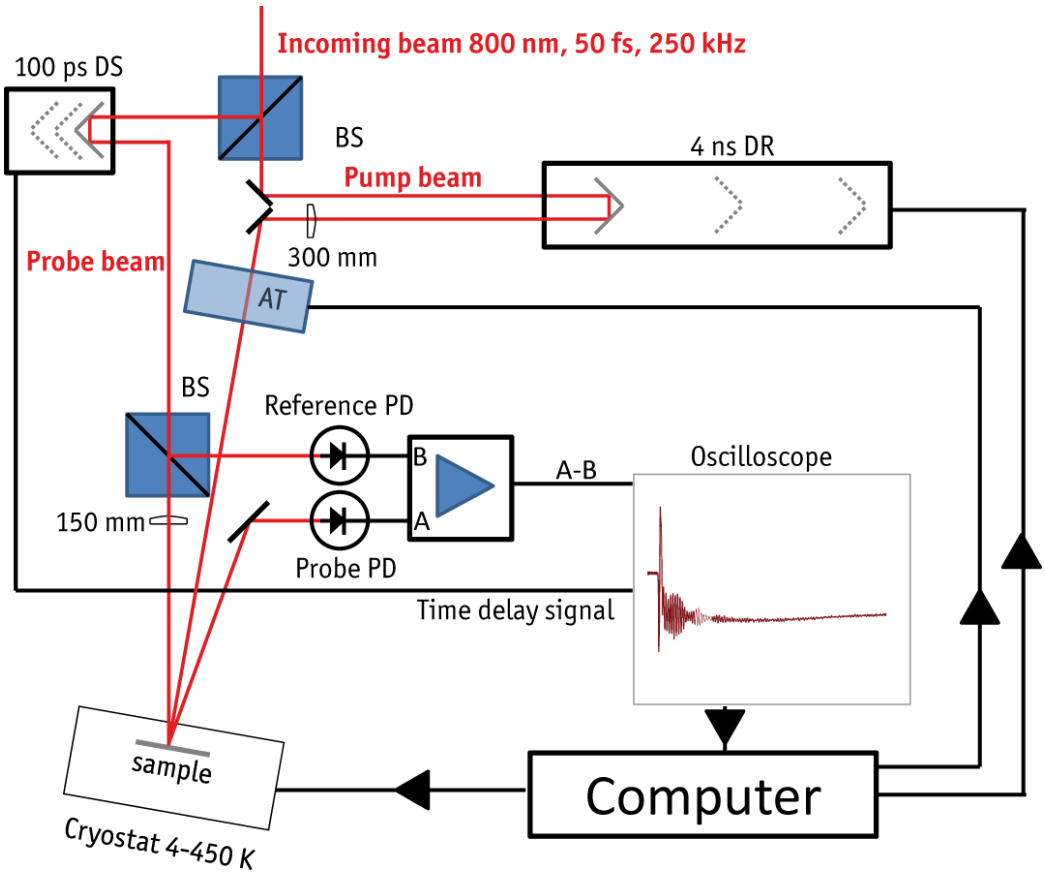

Fig. 1: Simplified scheme of the fully automatic setup that was used to retrieve the time resolved pump probe data. BS: beam splitter, PD: photo diode, DS: delay shaker, DR: delay stage, AT: attenuator, A: probe signal, B: reference signal.

2. Raman and IR active q=0 modes in the CDW state obtained within the TDGL model

The main motivations to apply the TDGL analysis in different limiting cases (adiabatic to non-adiabatic) are the observation of an overdamped (electronic) mode, whose damping time shows critical slowing down at T_c, the incomplete softening of several low frequency modes, as well as the peculiar temperature dependence of the damping of the phonon modes. As far as an overdamped electronic mode is concerned, we can easily rule out other alternative explanations. If this component was due to simple electron-phonon thermalization [1], no temperature dependence should be observed in contrast to experimental results. Alternatively, if this was an

overdamped phonon mode, the damping should increase with temperature and not decrease as observed.

As has been shown in the main text we can write the free energy as

$$\varphi = \varphi_0 + \frac{1}{2}\alpha(T - T_{c0})(\Delta_1^2 + \Delta_2^2) + \frac{1}{4}\beta(\Delta_1^2 + \Delta_2^2)^2 + \frac{\Omega_0^2}{2}(\xi_1^2 + \xi_2^2) - m(\Delta_1\xi_1 + \Delta_2\xi_2)\,. \quad (1)$$

Assuming small fluctuations near their equilibrium positions, the equations of motion of the EOP and the phonon mode are derived. The equations for the real parts of the order parameter (x_1,y_1), describing the overdamped amplitude mode of the electronic channel and the Raman active (symmetric) lattice vibration, respectively, are:

$$\begin{aligned} \dot{x}_1 &= -2\kappa\alpha(T_c + \frac{m^2}{2\alpha\Omega_0^2} - T)x_1 - \kappa m y_1 \\ \ddot{y}_1 &= -\Omega_0^2 y_1 - m x_1 \end{aligned} \quad (2)$$

The corresponding equations of motion for the two infrared active modes are:

$$\begin{aligned} \dot{x}_2 &= -\kappa\frac{m^2}{\Omega_0^2}x_2 - \kappa m y_2 \\ \ddot{y}_2 &= -\Omega_0^2 y_2 - m x_2 \end{aligned} \quad (3)$$

Equations (2),(3) describe the overdamped electronic relaxation channel and Raman and infrared (IR) active lattice vibrations, respectively. Clearly, each phonon mode at $\pm 2k_F$ (in the high temperature phase) generates in the low temperature phase one Raman active and one infrared active mode with the frequencies close to $\omega(2k_f)$ in agreement with [2]. Moreover, comparison of the equations (2) and (3) directly reveals that at T_c the IR mode frequency and damping are equal to that of the Raman active mode. Unlike for the case of the Raman active mode, the IR active mode shows no temperature dependence in the first approximation (see Eq.(3)). One should keep in mind, however, that as soon as there is some coupling between the IR and Raman modes (e.g. via higher order gradient terms of the order parameter in the thermodynamic potential) equations (2) and (3) become coupled.

Frequencies and dampings of the Raman active modes are determined by the equation:

$$\lambda^3 + 2\kappa\alpha(T_c - T + \frac{m^2}{2\alpha\Omega_0^2})\lambda^2 + \Omega_0^2\lambda + 2\kappa\alpha\Omega_0^2(T_c - T) = 0 \quad (4)$$

It is interesting to recover the standard amplitude and phase modes from this equation. If we assume that the electronic part is fast and adiabatically follows the lattice coordinates, i.e. $\kappa \to \infty$, we obtain the standard result for the temperature dependence of the amplitude mode as $\Omega \to 0$ as $T \to T_c$. With $\kappa \to \infty$, we can neglect the cubic and linear terms in (4) and obtain:

$$\Omega = \Omega_0 \sqrt{\frac{T_c - T}{T_c + \frac{m^2}{2\alpha\Omega_0^2} - T}} \qquad (5)$$

Similarly, for $\kappa \to \infty$ and putting $T=T_c$ (which transforms Eq. (4) to the equation for the infrared mode) leads to the known result that the phase mode is gapless with 0 frequency at *k=0* [3].

2.1. The temperature dependence of the mode frequency and damping

The most interesting parameter in our context is temperature. As follows from Eq. (4) at $T = T_c$ $\lambda_1^{(1)} = 0$ indicating that the relaxation time for the overdamped electronic mode diverges. On the other hand, the phonon frequency shows softening in most of the temperature range, while in the close vicinity of T_c it increases towards T_c.

The theory is in general applicable both in adiabatic and non-adiabatic limits (in the adiabatic limit the electron system adiabatically follows the lattice motion, while in the extreme non-adiabatic limit the electronic damping becomes slower than the inverse phonon frequency). However, in the close vicinity of T_c the model is expected to fail, since in this case fluctuation, which are not included in the model, become important. Formally, the validity of the Ginzburg-Landau theory is limited to the temperature range:

$$Gi \ll \left| \frac{T - T_c}{T_c} \right| \ll 1, \qquad (6)$$

where *Gi* is the Ginzburg number [4]. *Gi* is denoting the range where fluctuation of the order parameter are large, i.e. when $\left|\langle\Delta\rangle\right| < \sqrt{\langle\Delta^2\rangle - \langle\Delta\rangle^2}$. Therefore, the solutions plotted in Figs. 2 and 3 become invalid in the close vicinity of T_c.

In Fig. 2 the temperature dependence of the damping of the electronic mode and frequency and damping of the linearly coupled phonon mode is shown for different values of the bare electronic damping.

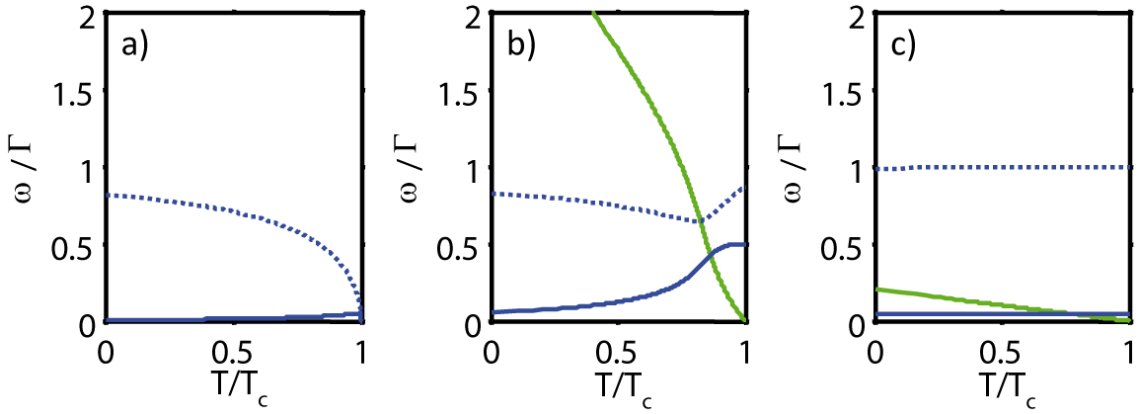

Fig. 2: The temperature dependence of the solution (green line: damping of the electronic mode, dotted blue line: phonon mode frequency, and solid blue line damping of the phonon mode). These are shown for different limiting cases: a) Adiabatic scenario: Strong electronic damping (Γ_e=10•Ω_0 – not shown, out of scale) leads to true soft mode behavior. b) Intermediate regime: Electronic damping of the order of the mode frequency (Γ_e=Ω_0) leads to mode softening at lower temperatures. Near T_c, when electronic damping becomes too slow (near T_c) the mode hardens again. c) Fully non-adiabatic case (Γ_e=0.1Ω_0): Only very weak hardening of the phonon mode is observed.

3. Extending the model to multiple phonons: numerical analysis

Starting from equation (1) we can extend this model to more than only one phonon mode by introducing a sum over all phonon modes *i*. We are considering only the symmetric Raman modes (IR modes are decoupled from Raman modes as shown above). The free energy is then given by:

$$(7) \qquad \phi = \phi_0 + \frac{\alpha}{2}(T - T_{c0})\Delta^2 + \frac{\beta}{4}\Delta^4 + \sum_i \frac{\Omega_i^{\,2}}{2}\xi_i^{\,2} - m_i \Delta \xi_i \ .$$

Here m_i are the coupling constants of the modes, while Ω_i are the mode frequencies and ξ_i the mode amplitudes. (Note that in this case the index *i* denotes the mode quantum number.)

This leads to a system of linear differential equations similar to Equation (2). To solve the system of linear differential equations numerically we reduce the system to the

system of first order differential equations by introducing dummy variables. E.g. Equation (2) is rewritten as (ψ is the dummy variable for the derivative of *y*):

$$
\begin{aligned}
&\dot{x} = -2\kappa\alpha\left(T_c + \frac{m^2}{\alpha\Omega_0{}^2} - T\right)x - \kappa m y \\
&\dot{y} = \psi \\
&\dot{\psi} = -\Omega_0{}^2 y - m x
\end{aligned}
\qquad (8)
$$

Searching for the solution of Eqs.(8) in the form $v = \tilde{v}_0 e^{\lambda t}$, where $\tilde{v}_0$ is the complex amplitude of the variables *x*, *y* , ψ, we obtain the eigenvalue equation

$$
\begin{aligned}
&\lambda\tilde{x}_0 = -2\kappa\alpha\left(T_c + \frac{m^2}{\alpha\Omega_0{}^2} - T\right)\tilde{x}_0 - \kappa m\tilde{y}_0 \\
&\lambda\tilde{y}_0 = \tilde{\psi}_0 \\
&\lambda\tilde{\psi}_0 = -\Omega_0{}^2\tilde{y}_0 - m\tilde{x}_0
\end{aligned}
\qquad (9)
$$

The eigenfrequencies and dampings may be calculated numerically as eigenvalues of the matrix:

$$
\begin{pmatrix}
-2\kappa\alpha\left(T_c + \dfrac{m^2}{\alpha\Omega_0{}^2} - T\right) & -\kappa m & 0 \\
0 & 0 & 1 \\
-m & -\Omega_0{}^2 & 0
\end{pmatrix}. \qquad (10)
$$

Eq. (9) corresponds to the previous case described by the cubic equation - Eq. (4).
For multiple phonons the system of equations of motion is written as:

$$
\begin{aligned}
&\dot{x} = -2\kappa\alpha\left(T_c + \frac{m_1{}^2}{\alpha\Omega_1{}^2} + \frac{m_2{}^2}{\alpha\Omega_2{}^2}\ldots - T\right)x - \kappa m_1 y_1 - \kappa m_2 y_2 \ldots \\
&\dot{y}_1 = \psi_1 \\
&\dot{\psi}_1 = -\Omega_1{}^2 y_1^1 - m_1 x \\
&\dot{y}_1^2 = \psi_1^2 \\
&\dot{\psi}_2 = -\Omega_2{}^2 y_2 - m_2 x \\
&\ldots.
\end{aligned}
\qquad (11)
$$

where the indices represent the phonon mode quantum numbers.
Transforming Eqs. (11) to the matrix form similar to Eqs. (9),(10) we obtain the eigenvalue equation of 1+2N order, where N is the number of phonon modes coupled to the EOP. For N>1 this equation is analyzed numerically. Even for N=1 the solution of the eigenvalue equation away from T_c is not straight forward.

In Fig. 3) we present an example of two phonon modes coupled linearly to the EOP. The coupling strength is the same for both modes, but the bare phonon frequencies are different for the three subplots. All plots shown are in the intermediate regime where ($\Gamma_e \approx \Omega_0$).

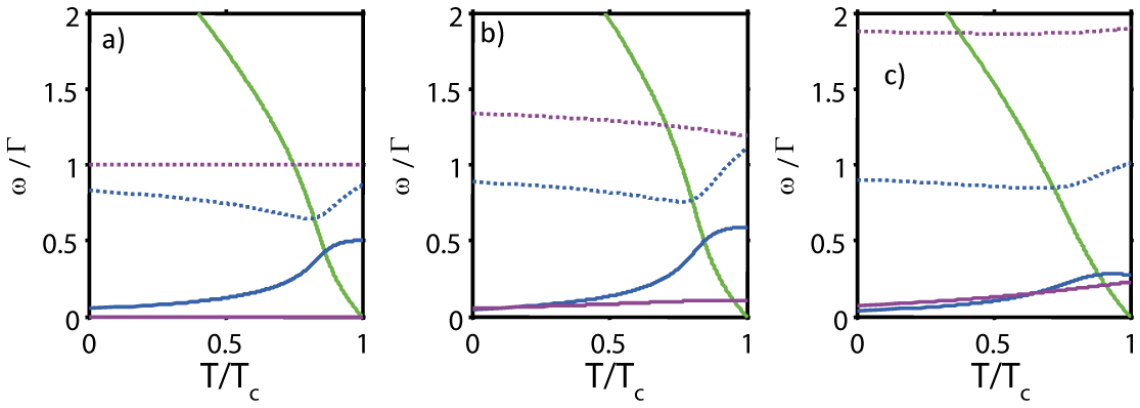

Fig. 3: Two phonons coupled linearly to the electronic part of the order parameter. a) Two modes with the same frequency ($\omega_1=\omega_2=1$). b) Two modes with frequencies ($\omega_1=1$ and $\omega_2=1.5$). c) Two modes with frequencies ($\omega_1=1$ and $\omega_2=2$). (green line: damping of the electronic mode, dotted blue/violet line: phonon modes frequencies, and solid blue/violet lines damping of the phonon modes).

Panel a) of Fig. 3) shows two modes having the same bare frequency. As expected, one of the modes shows no temperature dependence of frequency and damping. (This is also true for more than two modes with the same frequency). In panel b) the ratio of the bare frequencies is 1.5. This provides two features: The high frequency mode shows softening throughout the entire temperature range, while the low frequency mode experiences an upturn which overcomes its bare frequency near T_c. If the modes are far separated from each other, as shown in panel c), interaction becomes weaker and the temperature dependence become less pronounced.

4. Phonon spectra probed with different probe polarizations with respect to the crystal axes

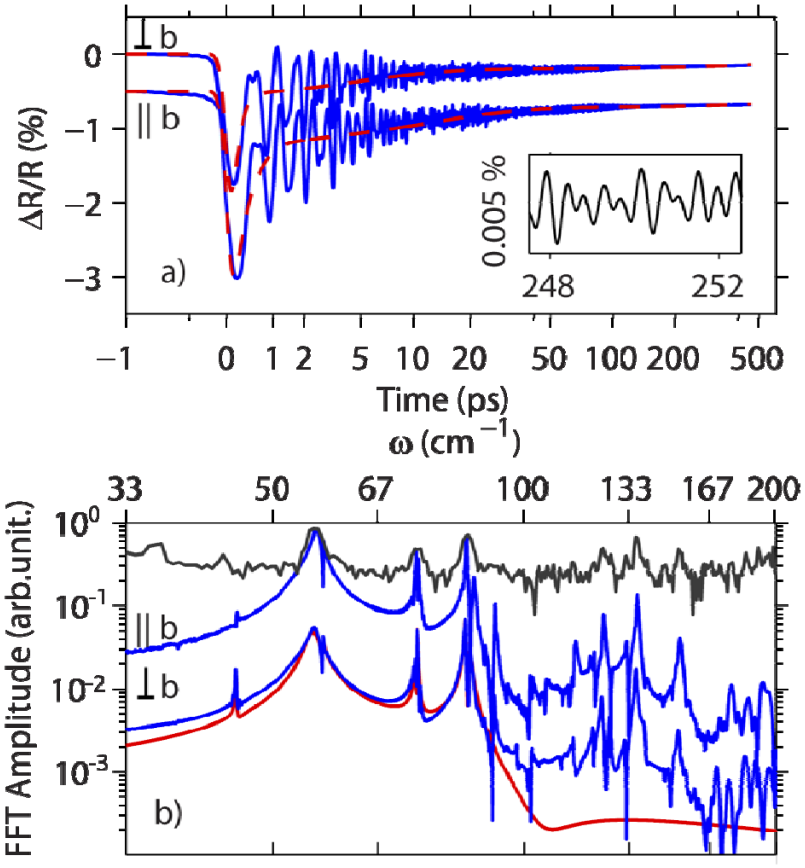

Fig.4: a) Comparison of the photoinduced reflectivity traces recorded at 10 K for both polarizations of the probe beam with respect to the crystal axes. b) The corresponding FFT spectra (amplitude). The red line is the fit accounting for modes at 1.36 THz (45.3 cm^{-1}), 1.68 THz (56 cm^{-1}), 1.72 THz (57.3 cm^{-1}), 2.21 THz (73.6 cm^{-1}), 2.23 THz (74.3cm^{-1}), 2.55 THz (85 cm^{-1}) and 2.58 THz (86 cm^{-1}).

Fig. 4 presents the comparison of the photoinduced reflectivity traces, recorded for both polarizations of the probe beam with respect to crystal axes, and their FFT (amplitude) spectra. We used a Lorentzian function to extract the characteristic parameters of the phonon modes:

$$\tilde{x}(\omega) = \frac{\tilde{x}_0}{\sqrt{(\omega_0 - \omega)^2 + \Gamma^2}} \qquad (12)$$

where $\tilde{x}_0$ is the complex amplitude, ω_0 the center frequency and Γ the phonon damping.

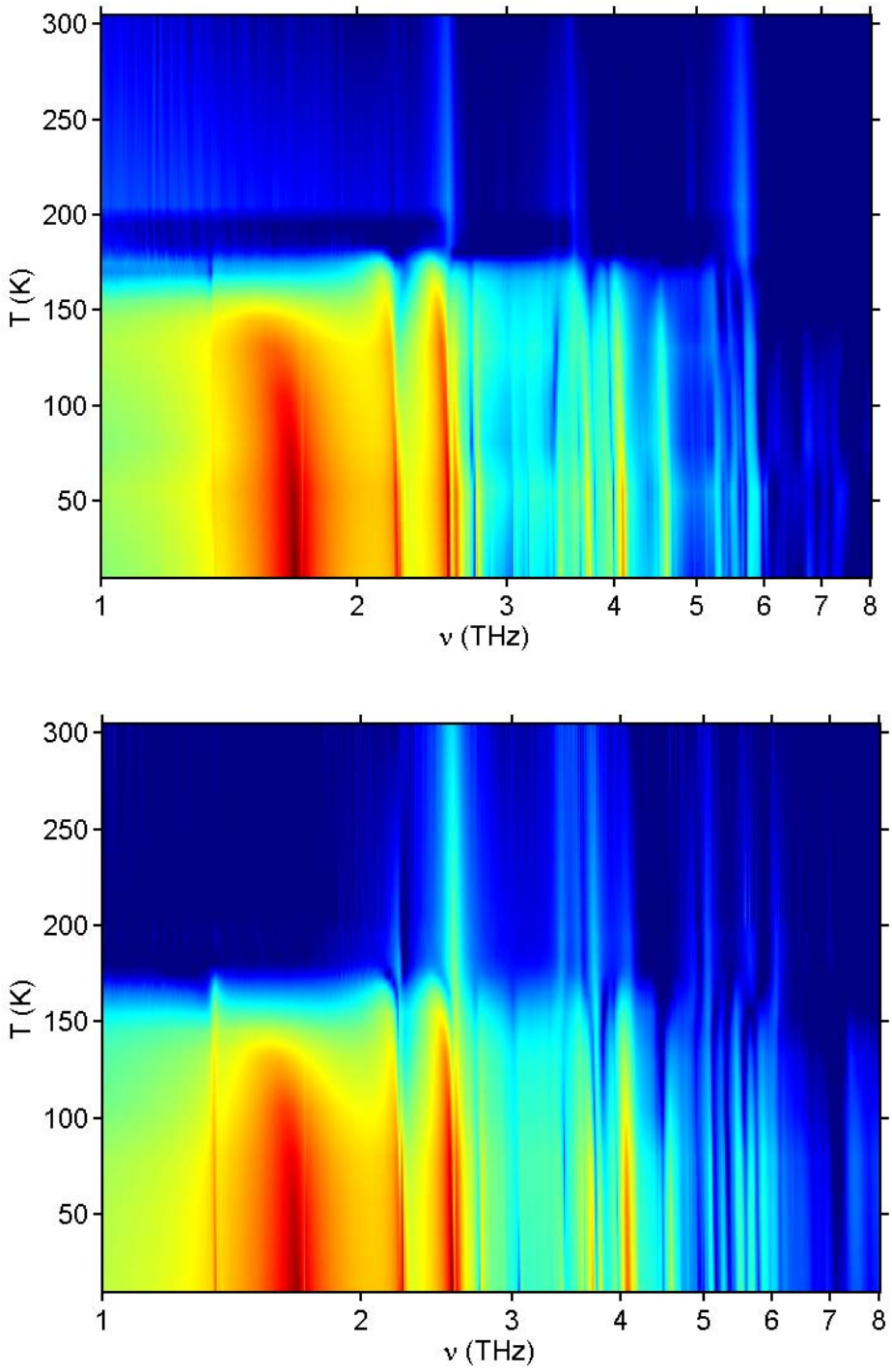

Fig. 5: The temperature dependent phonon spectrum probed with light polarized along the chain direction (b-axis) - top panel, and with probe light polarized perpendicularly to chain direction - bottom panel.

In both spectra (see Fig. 4 and Fig. 5 for their temperature dependencies) the main modes are at the same frequency and show the same temperature dependence. The weak satellite modes, which show almost no temperature dependence of their frequencies, are in general more pronounced in the configuration, where the probe polarization is perpendicular to chain direction. Moreover, the satellite modes at 2.58 THz as well as at 2.23 THz, are found to persist up to high temperatures, suggesting that they are the q=0 modes of the high temperature phase.

5. The temperature dependence of the phonon parameters

As discussed in the main text, the mode parameters were obtained by fitting the FFT data with the sum of Lorentzian line fits. Each line is determined by the four parameters: Amplitude, frequency, damping and phase. The amplitude, frequency and damping have been discussed in the manuscript. However, the damping was shown on the linear scale (given by bars in Fig. 2 of the main text). In Fig. 6 a) we show the temperature dependence of the corresponding decay times on the semi-log plot. Importantly, the temperature dependencies of the dampings of the modes cannot be accounted for by a standard anharmonic decay model - see dashed curves in Fig. 6 b), where for a phonon of energy $\hbar\omega_0$ the T-dependence of damping is given by $\Gamma(T)=\Gamma(0)\left(1+2/(e^{\hbar\omega_0/2k_BT}-1)\right)$ [5]. On the other hand $\Gamma(T)$ is well reproduced by our model – see solid lines in Fig. 6 b) – where single parameter (the coupling strength between the $2k_F$ phonon mode and the EOP) is used to describe both T-dependence of softening and damping (see Fig. 2 of the main text).

For completeness, we are showing in Fig. 7 also the T-dependence of the phases of the coherently excited modes. As was discussed by Stevens et al. [6], the coherent phonon generation can be described by the two stimulated Raman tensors. This model contains both, the so called "impulsive" [6,7] and "displacive" [8] limiting cases, where the phase in the pure "impulsive" limit is $\pi/2$, while in the pure "displacive" limit it is 0. At low temperatures, the main modes show cosine like dynamics (as in the "displacive" limit), where phase is close to 0. The phases change as the critical temperature is approached, in a quite dramatic way.

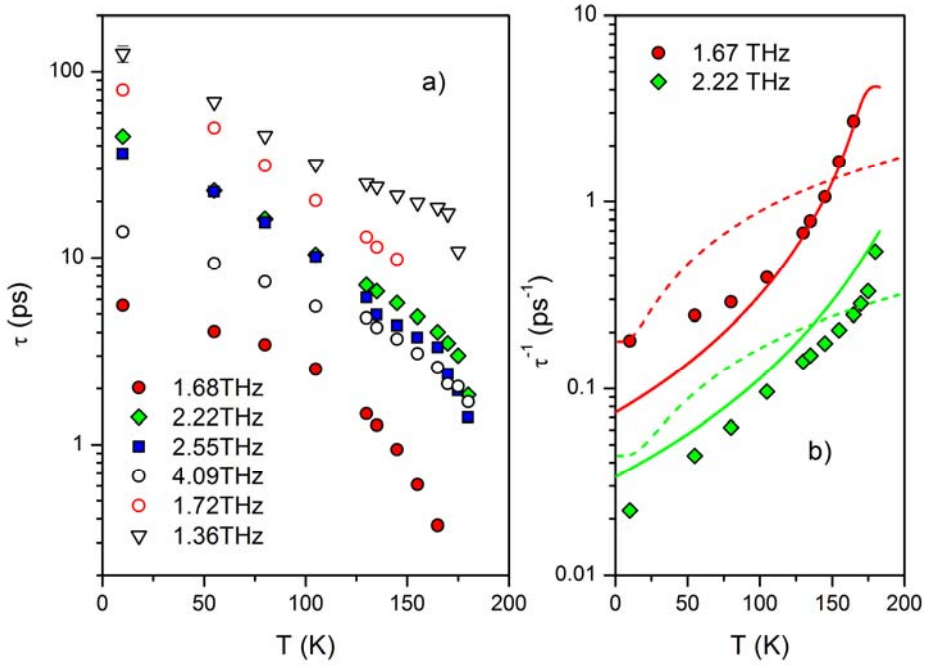

Fig. 6: a) The T-dependence of the decay times of the modes discussed in the main text. The error bars extracted from the fit are typically smaller than the symbol size, except for 1.36 THz mode at 10 K. b) The T-dependence of damping for two modes (1.68 and 2.22 THz) compared to the fit with the model (solid lines) and the standard anharmonic decay model (dashed lines).

For the general case (including both displacive and impulsive limits) the phase of the coherent phonon can be evaluated [9]. To be able to apply this model, however, one would need the data on the temperature dependence of the derivative of the real part of the dielectric function with respect to frequency at the optical frequency, which do not exist. Secondly, and more importantly, the modes that we are discussing are linearly (or even higher order - see Section 6) coupled to each other via the electronic part of the order parameter. It is most probably that the coupling between the modes, together with the strong temperature dependence of the dielectric function, and all the damping times, give such a dramatic temperature dependence of the phases. Given the fact, that these questions are far beyond the central topic of this paper, we are leaving this issue for future publication.

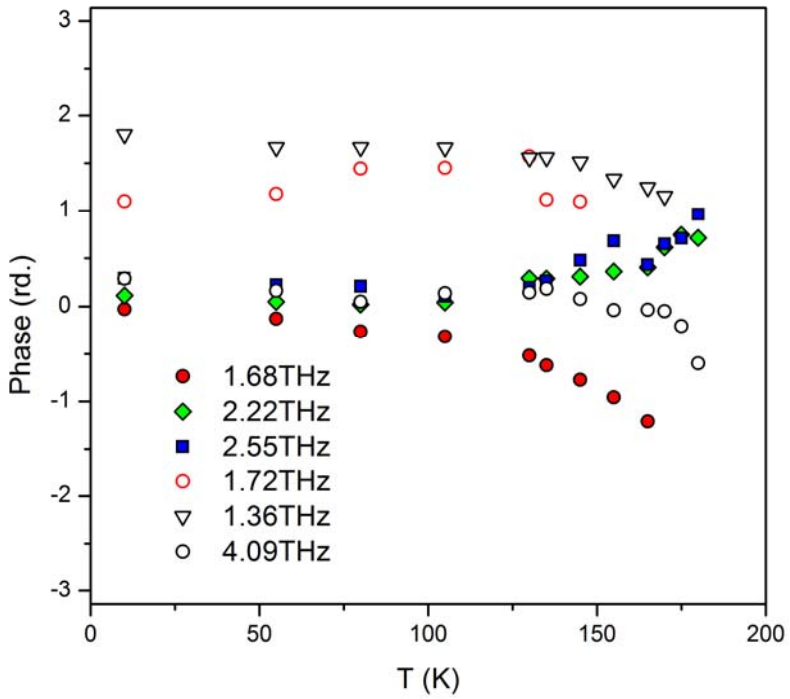

Fig. 7: The temperature dependency of the phase of the phonon modes, where each mode (*i*) follows $A_i * \exp(-t/\tau_i) * \cos(\omega_i t - \phi_i)$, where t is the time delay after photoexcitation. The error-bars for all the data points are about 0.2 rd., determined by the uncertainty of the zero time delay of about 20 fs.

6. On the possible nature of the narrow satellite modes

We should discuss the possible nature of narrow satellite modes which are located in the close vicinity of the main T-dependent modes and show no measurable T-dependence of frequency. As discussed above, the modes at 2.23 and 2.58 THz are, though very weak, observed also above T_c and can be therefore attributed to q=0 modes of the high temperature phase. The mode at 1.72 THz is, despite the extremely high sensitivity, not resolved above ≈ 150 K.

The modes that are present only below T_c could in principle arise due to higher order coupling to the electronic part of the order parameter; i.e. they could correspond to $4k_F$, $6k_F$ … phonons of the high temperature phase. Because of the higher order coupling to the electronic part of the order parameter one would expect that: a) their frequency shows much weaker temperature dependence and b) that their amplitude would be proportional to higher powers of the order parameter, $|\Delta|^4$,$|\Delta|^6$ … This explanation could well describe the mode at 1.72 THz.

The modes at 2.23 and 2.58 THz are observed also above T_c, suggesting that they are q=0 phonons of the high temperature phase. For the q=0 phonon, whose frequency lies in close proximity to the "folded" mode (the mode that results due to linear coupling to the electronic part of the order parameter), coupling to the folded mode is expected. This coupling could result in a substantial increase in the q=0 phonon intensity below T_c, as experimentally observed (See Fig. 5 for the 2.23 THz mode). In such a case, terms $(a_i + b_i|\Delta|^2)\zeta_i$ should be included in the expansion of the dielectric function (Eq.(4) of the main text), where ζ_i is the generalized phonon coordinate while a_i and b_i are constants (a_i is in general temperature dependent). Using the same argument as for the "folded" modes the resulting q=0 phonon amplitudes should show $(a_i + b_i|\Delta|^2)^2$ T-dependence. Indeed, as shown in Figure 8, amplitudes of 1.72 and 2.23 THz modes decreases much faster than for the case of "folded" modes. Red line presents the fit with $(a_1 + b_1|\Delta|^2)^2$, where a_1 was assumed to be T-independent. The fit shows a good agreement with the data.

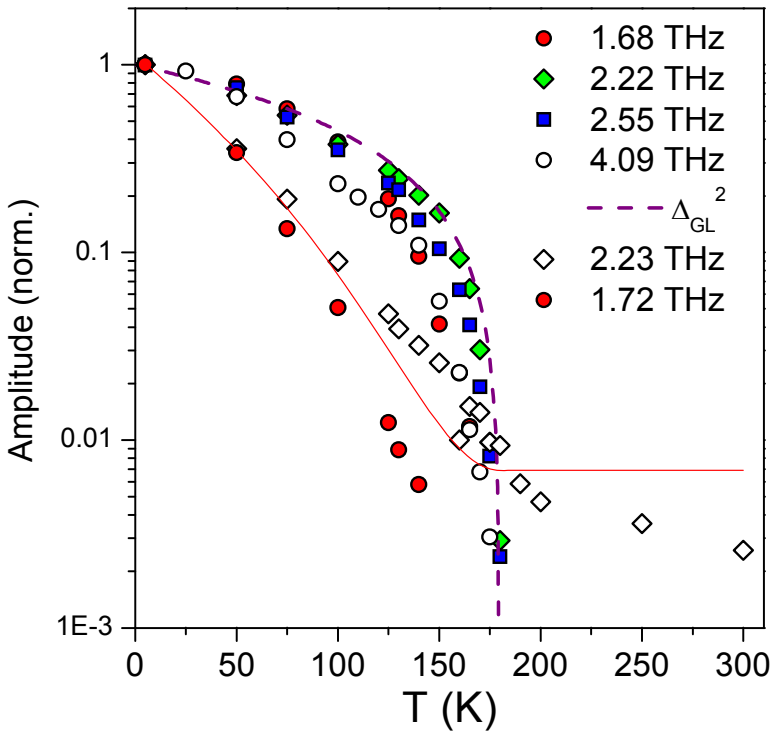

Fig. 8: The temperature dependence of the amplitudes of several phonon modes (normalized to their lowest temperature value). While the main modes follow the $|\Delta|^2$ temperature dependence, the amplitude of satellite modes decreases faster (see e.g. modes at 1.72 and 2.23 THz). The one for 2.23 THz mode can be well fit with $(a_1 + b_1|\Delta|^2)^2$ - red line (here a_1 was assumed to be temperature independent).

References

[1] see. e.g. R. H. M. Groeneveld, R. Sprik, and A. Lagendijk, Phys. Rev. B 51, 11433, (1991) and references therein.

[2] M.J. Rice, Phys. Rev. Lett., 36 (1976).

[3] G. Grüner, Density waves in Solids, Addison-Wesley, 1994.

[4] G. Klemens, Phys. Rev. 148, 845 (1966); M. Balkanski, R. F. Wallis and E. Haro, Phys. Rev. B 28, 1928 (1993).

[5] V. L. Ginzburg, Fizika Tverdogo Tela 2, 2031 (1960); Sov. Phys. Solid State 2, 1824 (1961).

[6] T. E. Stevens, J. Kuhl, and R. Merlin, Phys. Rev. B 65, 144304 (2002).

[7] L. Dhar, J.A. Rogers, K.A. Nelson, Chem. Rev. 94, 157 (1994);

[8] H.J. Zeiger et al., Phys. Rev. B 45, 768 (1992).

[9] D. M. Riffe and A. J. Sabbah, Phys. Rev. B 76, 085207 (2007)